

Decomposing and Routing Quantum Circuits Under Constraints for Neutral Atom Architectures

Natalia Nottingham^{1,*}, Michael A. Perlin², Ryan White¹, Hannes Bernien¹, Frederic T. Chong¹, and Jonathan M. Baker^{3,4}

¹University of Chicago, Chicago, Illinois, USA

²Inleqtion, Chicago, Illinois, USA

³Duke University, Durham, North Carolina, USA

⁴University of Texas at Austin, Austin, Texas, USA

ABSTRACT

Quantum computing is in an era defined by rapidly evolving quantum hardware technologies, combined with persisting high gate error rates, large amounts of noise, and short coherence times. Overcoming these limitations requires systems-level approaches that account for the strengths and weaknesses of the underlying hardware technology. Yet few hardware-aware compiler techniques exist for neutral atom devices, with no prior work on compiling to the neutral atom native gate set. In particular, current neutral atom hardware does not support certain single-qubit rotations via local addressing, which often requires the circuit to be decomposed into a large number of gates, leading to long circuit durations and low overall fidelities.

We propose the first compiler designed to overcome the challenges of limited local addressability in neutral atom quantum computers. We present algorithms to decompose circuits into the neutral atom native gate set, with emphasis on optimizing total pulse area of global gates, which dominate gate execution costs in several current architectures. Furthermore, we explore atom movement as an alternative to expensive gate decompositions, gaining immense speedup with routing, which remains a huge overhead for many quantum circuits. Our decomposition optimizations result in up to $\sim 3.5x$ and $\sim 2.9x$ speedup in time spent executing global gates and time spent executing single-qubit gates, respectively. When combined with our atom movement routing algorithms, our compiler achieves up to $\sim 10x$ reduction in circuit duration, with over $\sim 2x$ improvement in fidelity. We show that our compiler strategies can be adapted for a variety of hardware-level parameters as neutral atom technology continues to develop.

1. INTRODUCTION

Recent years have shown drastic improvements in the development of quantum computing hardware technologies, including superconducting qubits, neutral atoms, and trapped

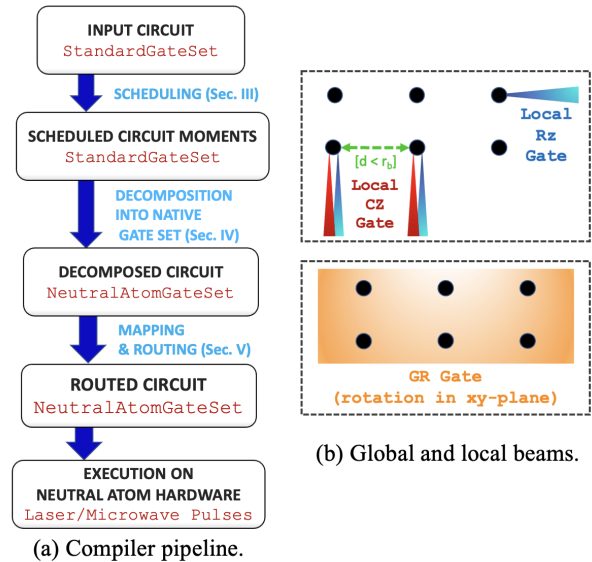


Figure 1: (a) Compiler pipeline for converting a high-level quantum program into a circuit that can be executed on neutral atom hardware. (b) Recent neutral atom devices support local-addressability for Rz and CZ gates, but not for single-qubit rotations in the xy-plane. CZ gates can act on qubit pairs with a separation distance smaller than the blockade radius.

ions. Neutral atom quantum computers have demonstrated immense promise due to their exceptionally long coherence times, scalability, native multi-qubit gates, higher connectivity resulting from longer-range interactions, and the ability to produce identical and well-characterized qubits [12, 17].

Despite these advancements, quantum computing remains in an era defined by large amounts of noise, high gate error rates, and the possibility of qubit states decohering prior to completion of the circuit. Given these constraints, hardware-aware optimizations at the compiler level—that successfully exploit the hardware platform’s advantages while employ-

*nottingham@uchicago.edu

ing techniques to overcome its limitations—are absolutely essential. At the same time, since neutral atoms are a newer and rapidly evolving hardware platform, we need compiler approaches that can be easily applied to a wide variety of hardware models as the technology grows.

While considerable prior work exists on quantum compilation [1, 6, 7, 16, 18, 23, 26], the majority of such work has either been hardware-agnostic or tailored to the constraints of superconducting qubits, with limited work focusing on compiler approaches for neutral atoms. Baker et al. [2], Patel et. al. [19], and Li et. al. [15] took the first steps towards developing compilers specific to neutral atom hardware, accounting for properties such as long-distance interactions, atom loss, and native multi-qubit gates.

However, [2, 15, 19] assume a native gate set in which all single-qubit gates can be executed via locally-addressing beams. This assumption is inconsistent with current neutral atom hardware, where execution of certain single-qubit gates is only supported natively via globally-addressing beams that rotate all qubits homogeneously. Though global addressing presents fewer engineering challenges and lower costs on a hardware level, it creates a more difficult compiler problem: if a global gate is used to execute an operation that acts only on a small subset of qubits in the original circuit, the compiler must ensure that any operation on off-target qubits is “undone”. This consideration can lead to expensive decompositions and contributes significantly to circuit runtimes.

In this paper, we propose two main contributions to address this problem. First, we develop compiler passes to decompose a high-level input quantum circuit, expressed in terms of any arbitrary gate set, into a native gate set that is realistic of current neutral atom hardware with limited local control. We significantly reduce the cost of the single-qubit gate decompositions by minimizing the total global gate pulse area, with additional optimizations to lower R_z gate costs.

Second, we observe that a large number of native neutral atom gates is required to decompose each SWAP gate, greatly increasing routing overhead when using conventional SWAP-based routing strategies on neutral atom devices. We therefore develop routing methods that incorporate atom movement as an alternative to expensive SWAP decompositions. Because physical rearrangement of atoms is not limited by blockade radius, it provides a strong alternative to SWAP gates, allowing us to overcome device connectivity constraints and providing greater flexibility in routing decisions. Our approach greatly lowers two-qubit gate costs and routing overhead, improving both circuit duration and fidelity.

We combine these steps into a full compiler pipeline designed to overcome the challenges of global addressing while exploiting the benefits of atom movement. Our specific contributions are the following:

- Two decomposition methods, including optimizations that minimize the global rotation angle necessary to decompose a collection of parallel single-qubit gates, resulting in up to 3.5x improvement in total global gate execution time.
- A routing algorithm using atom movement that achieves 2.5x average speedup in circuit duration across all

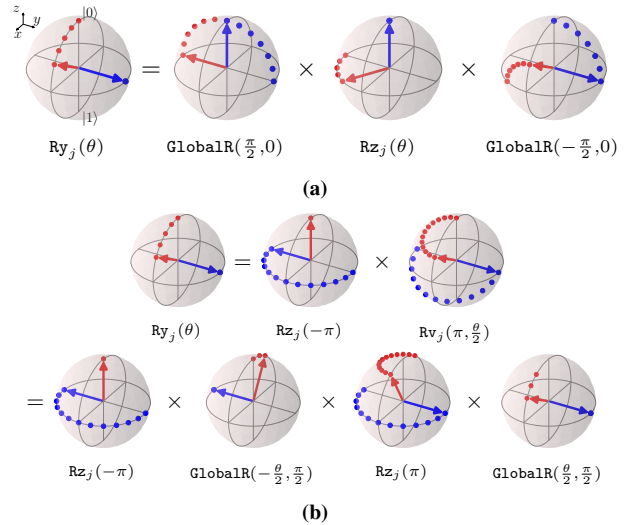


Figure 2: Two decompositions of a local gate that rotates qubit j about the Y axis by an angle θ . Red and blue arrows track the trajectories of states initially pointing along the $+z$ and $+y$ axes on the Bloch sphere, respectively corresponding to the initial states $|0\rangle$ and $|0\rangle + i|1\rangle$. (a) Axial decomposition of a local R_y gate, which uses global pulses to swap the Y and Z axes and imprints the rotation angle θ onto qubit j with a local (axial) R_z gate. This involves a net global rotation of π . (b) Transverse decomposition of a local R_y gate, which uses global pulses to swap the $V_{\theta/2}$ and Z axes, thereby imprinting the rotation angle θ onto qubit j with global (transverse) GR gates. This involves a net global rotation of $|\theta| \leq \pi$.

benchmarks and hardware models tested, with this number increased to 3.5x average speedup on hardware where global gate durations are dominant.

- A holistic pipeline (shown in Figure 1) that, when all components are combined, achieves up to 10x speedup and 2x improvement in fidelity.
- Evaluations which account for several key hardware-level parameters, demonstrating that our compiler passes can be successfully applied to a diverse set of neutral atom hardware models.

2. BACKGROUND

2.1 Quantum Computing

The state of quantum bits, or *qubits*, is represented as a complex linear superposition $\alpha|0\rangle + \beta|1\rangle$ of the single-qubit basis states $|0\rangle$ and $|1\rangle$. This state is manipulated by gates; an n -qubit gate is represented by a $2^n \times 2^n$ unitary matrix. All single-qubit quantum gates can be visualized as rotating the state by a given angle around a specified axis on the Bloch sphere, where the unit vectors along the sphere’s $+z$ and $-z$ axes represent the computational basis states $|0\rangle$ and $|1\rangle$, respectively. Examples of these rotations are in Figure 2.

2.2 Native Gate Set & Global Addressing

At a high level, a quantum program is expressed in terms of operations from a chosen universal gate set, usually consisting of arbitrary $U3$ single-qubit rotations plus a two-qubit entangling gate such as CZ. We refer to this gate set $\{U3, CZ\}$ as the `StandardGateSet`. However, this may contain operations are not in the hardware’s *native gate set*, i.e., the set of gates that can be directly executed on hardware, usually in the form of laser or microwave pulses. The compiler must convert high-level quantum circuits into an equivalent circuit using only gates from the hardware’s native gate set.

Current neutral atom technology does not natively support individually-addressing single-qubit rotations about an axis in the xy -plane of the Bloch sphere, where *individually-addressing* or *locally-addressing* gates refer to operations applied to a chosen qubit without affecting other qubits. Instead, *globally-addressing* gates must be used where the same operation is applied simultaneously to all qubits in the circuit.

The neutral atom native gate set we consider is referred to as the `NeutralAtomGateSet`, consisting of local CZ gates, local $Rz(\lambda)$ gates, and global $GR(\theta, \phi)$ gates:

$$CZ = \text{diag}(1, 1, 1, -1), \quad (1)$$

$$Rz(\lambda) = \exp(-i\lambda\hat{Z}/2) = \text{diag}(e^{-i\lambda/2}, e^{i\lambda/2}), \quad (2)$$

$$GR(\theta, \phi) = \exp\left(-i\frac{\theta}{2}\sum_{j=1}^n(\cos(\phi)\hat{X}_j + \sin(\phi)\hat{Y}_j)\right). \quad (3)$$

Here, \hat{Z} is a single-qubit Pauli-Z matrix, \hat{X}_j and \hat{Y}_j are Pauli-X and Pauli-Y matrices for qubit j , λ and θ are rotation angles for Rz and GR gates, and the angle ϕ parameterizes the GR gate’s axis of rotation. The globally-addressing $GR(\theta, \phi)$ gate implements the same operation as n locally-addressing $R(\theta, \phi)$ gates executed separately on each qubit in the circuit.

When decomposing to a gate set containing global operations, there is the potential for significant increases in the circuit’s total gate count (see Section 3). Optimizing this step is crucial to maximizing performance and fidelity.

2.3 Atom Movement

One advantage of neutral atoms is the ability to physically move qubits from one location to another during execution of the circuit. In contrast, with superconducting hardware, for example, physical qubits must remain in a fixed location on the hardware, and quantum states stored in the qubits are exchanged via gate-level SWAP operations: $SWAP(|\psi_1\rangle \otimes |\psi_2\rangle) = |\psi_2\rangle \otimes |\psi_1\rangle$. Bluvstein et al. [4] show experimentally that entangled qubits can be coherently transported across a two-dimensional atom array with no negative effect on qubit entanglement nor fidelity when qubits are moved at a speed of $0.55\mu\text{m}/\mu\text{s}$ or slower. Though atom loss was noted to be the dominant error source with atom movement, this did not begin to have any effect until movement speed was increased beyond the threshold of $0.55\mu\text{m}/\mu\text{s}$. This ability to rearrange atoms mid-experiment creates the possibility of changing the connectivity of the atomic array, enabling higher levels of control over how and when CZ and Rz gates are applied.

2.4 Neutral Atom Hardware

With neutral atom quantum computing, the computational states $|0\rangle$ and $|1\rangle$ are encoded in the hyperfine ground states of an alkali atom such as Cesium (Cs) or Rubidium (Rb),

or alkaline-earth atom such as Strontium (Sr) or Ytterbium (Yb). Two-qubit entangling interactions are mediated with highly-excited Rydberg states [20]. CZ and Rz gates are implemented via locally-addressing beams involving a blue-wavelength laser – which off-resonantly addresses an atomic transition between the computational $|0\rangle$ state and an intermediate state – and an infrared laser, which bridges the excitation from the intermediate state to a Rydberg state. Simultaneous application of both the blue and infrared lasers on two nearby qubits is used to achieve a CZ gate if the qubits are within a “blockade radius”, i.e., if they are close enough that excitation to the Rydberg state in one atom shifts the Rydberg transition to be off-resonant in the other atom. Application of the blue laser alone induces an AC Stark shift, which shifts the $|0\rangle$ and $|1\rangle$ energy levels relative to each other without changing the state populations, thereby accomplishing a single-qubit Rz gate. Single-qubit Rx and Ry gates, which change the $|0\rangle$ and $|1\rangle$ state populations, require a different infrastructure, implemented via globally-addressing microwaves introduced with a microwave horn [10] or Raman laser system [14].

Atoms are held in place within a two-dimensional array by optical tweezers, generated using e.g. a spatial light modulator (SLM). Acousto-optic deflectors (AODs) rearrange atoms within the array [4], with one AOD controlling horizontal movement and another controlling vertical movement. While SLMs allow for any arbitrary two-dimensional arrangement of atoms, certain arrangements work better than others with AOD constraints; specifically, grid-like patterns allow for greater parallelism of movement operations. Spacing between atom sites is usually between $\sim 2\text{-}10\mu\text{m}$ [11, 22].

2.5 Related Work & Motivation

Numerous works exist on general quantum compilers or those tailored to superconducting systems, including [1, 6, 7, 16, 18, 23, 26]. However, none of these frameworks support atom movement operations in circuits nor decompositions involving GR gates. Both components are important in neutral atom systems, and modifying previous frameworks to incorporate these components is not trivial.

Baker et al. [2] proposed the first compiler to account for hardware-level characteristics specific to neutral atom devices, including long-distance interactions and atom loss. Patel et al. [19] expanded upon this work with compiler strategies to replace one- and two-qubit circuit blocks with native three-qubit gates, thereby reducing total pulse count. Li et al. [15] developed scheduling techniques based on connectivity and parallelism constraints in neutral atom computers. Note that these works cannot be directly compared to our work in evaluations because they assume local addressibility for every gate. To execute circuits on hardware, their compilers would require additional passes (such as those implemented in our work) to decompose into a more realistic neutral atom native gate set.

Tan et al. [24] developed the first compiler to incorporate atom movement into the routing step. While they provide a strong first step to build upon, particularly with accounting for hardware-level constraints at the compiler level, their algorithm is not scalable to larger circuits. Additionally, their approach requires a very large space overhead, which also leads to high atom movement costs, as atoms must travel

farther distances. Their work minimizes two-qubit gate costs, but further work is needed to reduce atom movement costs.

3. DECOMPOSING TO NATIVE GATES

3.1 Pre-Processing

We assume every circuit has been “pre-compiled” by commuting any sequence of single-qubit Rz gates past two-qubit CZ gates to merge Rz gates with other single-qubit gates. Additionally, the circuit must be transpiled into the `StandardGateSet` of {U3, CZ}. Existing transpiler passes from `Qiskit` or `Cirq` are sufficient for this [1, 7].

Before applying the decomposition steps, the circuit must be scheduled such that each moment contains either a) a group of parallelizable U3 gates or b) a group of parallelizable CZ gates; i.e., a U3 gate and CZ gate cannot be scheduled into the same moment. Using the decompositions presented below, any collection of parallelizable single-qubit gates can be decomposed together using the same number of global gates required to decompose only one single-qubit gate. Thus, maximizing single-qubit gate parallelism prior to decomposition minimizes the number of global gates in the final circuit.

Note that if routing occurs prior to decomposing into the native gate set, the circuit that is input into decomposition step can also contain movement operations, which can be scheduled into the same moments as CZ gates.

3.2 Axial Decomposition

Next, we decompose collections of parallelizable single-qubit gates from the `StandardGateSet` into the `NeutralAtomGateSet`. We begin by decomposing any single-qubit U3 gate into Euler-angle rotations as

$$\text{U3}(\theta, \phi, \lambda) = \text{Rz}(\phi) \text{Ry}(\theta) \text{Rz}(\lambda), \quad (4)$$

where Rz and Ry are single-qubit rotations about the z and y axes. The Rz gate is already an element of the `NeutralAtomGateSet`, so we only need to decompose the Ry gate further.

In the `axial` decomposition, the single-qubit Ry gates are decomposed into the form

$$\prod_j \text{Ry}_j(\theta_j) = \text{GR}\left(-\frac{\pi}{2}, 0\right) \left[\prod_j \text{Rz}_j(\theta_j) \right] \text{GR}\left(\frac{\pi}{2}, 0\right), \quad (5)$$

where $\text{Ry}_j(\theta_j)$ and $\text{Rz}_j(\theta_j)$ are respectively Ry and Rz gates addressing qubit j . This decomposition is visualized in Figure 2(a). Intuitively, this decomposition uses a GR gate to move the y axis to the z axis, rotates qubits about the z axis with local Rz gates, and then moves the z axis back to the y axis with another GR gate.

3.3 Transverse Decomposition

The key feature of the `transverse` decomposition, as compared to the `axial` decomposition presented above, is that it has a net GR pulse area of $|\theta|$ rather than π , which is the minimum GR pulse area possible to implement an $\text{Ry}(\theta)$ gate. This minimization results in significantly reduced run-times in hardware platforms that implement the GR gates with relatively slow microwave beams.

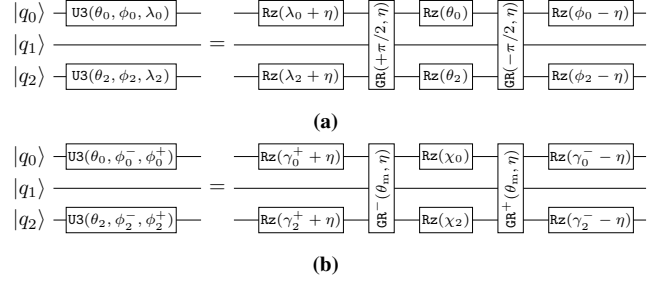


Figure 3: A `StandardGateSet` moment of single-qubit gates decomposed into the `NeutralAtomGateSet` using (a) `axial` decomposition and (b) `transverse` decomposition. Here $\text{GR}^\pm(\theta_m, \eta) = \text{GR}(\pm\theta_m/2, \pi/2 + \eta)$ and $\theta_m = \pm \max_j |\theta_j|$ for shorthand. In this example, the global rotations in both decompositions cancel on qubit q_1 , which has no gate acting on it in the original moment.

We start by once again decomposing the single-qubit U3 gate into Euler angles according to 4. The difference comes from our decomposition of the single-qubit Ry gate, which relies on the decomposition of a rotation into two reflections:

$$\text{Ry}(\theta) = \text{Rv}\left(\pi, \frac{\theta}{2}\right) \text{Rz}(-\pi) \quad (6)$$

where $\text{Rv}(\xi, \omega)$ is a single-qubit rotation by the angle ξ about the axis $\mathbb{V}_\omega = \cos \omega \mathbb{Z} + \sin \omega \mathbb{X}$. In turn, we can decompose

$$\text{Rv}(\xi, \omega) = \text{GR}\left(\omega, \frac{\pi}{2}\right) \text{Rz}(\xi) \text{GR}\left(-\omega, \frac{\pi}{2}\right). \quad (7)$$

This decomposition is visualized in Figure 2(b). Similarly to the `axial` decomposition, this decomposition can be understood as moving the \mathbb{V}_ω axis to the z axis, rotating about the z axis, and moving the z axis back to \mathbb{V}_ω .

Putting everything together, when multiple qubits are addressed by U3 gates the `transverse` decomposition takes the form

$$\prod_j \text{U3}_j(\theta_j, \phi_j^-, \phi_j^+) = \prod_j \text{Rz}_j(\gamma_j^-) \text{Rv}_j\left(\chi_j, \frac{\theta_{\max}}{2}\right) \text{Rz}_j(\gamma_j^+) \quad (8)$$

where $\theta_{\max} = \pm \max_j |\theta_j|$ (sign arbitrary), and the angles γ_j^+ , γ_j^- , and χ_j are defined in terms of arbitrary signs $\sigma_j \in \{+1, -1\}$ by

$$\gamma_j^\pm = \phi_j^\pm - \sigma_j(\alpha_j \pm \beta_j), \quad (9)$$

$$\alpha_j = \arctan(\cos(\theta_{\max}/2) \kappa_j), \quad (10)$$

$$\beta_j = \text{sign}(\theta_j) \text{sign}(\theta_{\max}) \times \frac{\pi}{2}, \quad (11)$$

$$\chi_j = \sigma_j \times 2 \arctan(\kappa_j), \quad (12)$$

$$\kappa_j = \sqrt{\frac{\sin(\theta_j/2)^2}{\sin(\theta_{\max}/2)^2 - \sin(\theta_j/2)^2}}. \quad (13)$$

Here $\text{sign}(x) = x/|x| \in \{+1, -1\}$ if $x \neq 0$ and 0 otherwise. We define $\kappa_j = \infty$ if $\theta_j = \pm \theta_{\max}$, with $\arctan(\infty) = \pi/2$. The axis of rotation for the GR gate can be changed with the

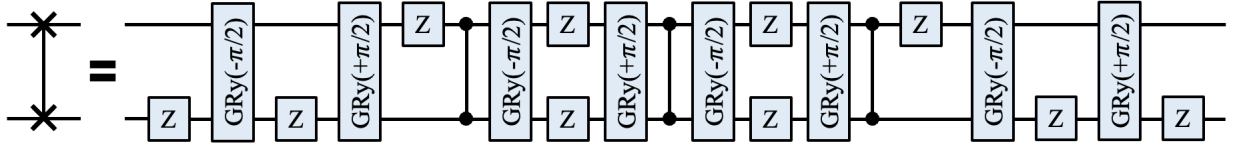


Figure 4: Decomposition of a single SWAP gate into the NeutralAtomGateSet. This is achieved by converting into CX gates, then into CZ and Hadamard gates: $\text{SWAP}(q_a, q_b) = \text{CX}(q_b, q_a) \cdot \text{CX}(q_a, q_b) \cdot \text{CX}(q_b, q_a)$ and $\text{CX}(q_a, q_b) = \text{H}(q_b) \cdot \text{CZ}(q_a, q_b) \cdot \text{H}(q_b)$. Each H is decomposed into the GR gates and Rz gates using methods from Sec. 3.3. We commute Pauli Z and CZ gates where doing so allows us to then cancel adjacent Pauli Zs on the same qubit.

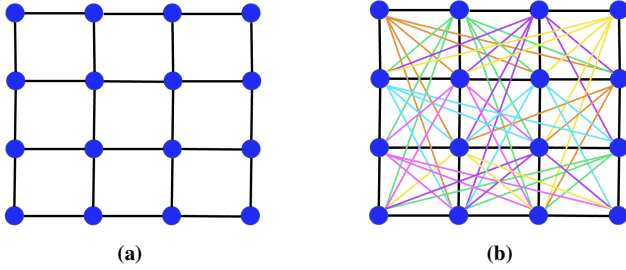


Figure 5: (a) Connectivity graph for blockade radius r_b and spacing s such that $s < r_b < s \cdot \sqrt{2}$. (b) Movement graph for the same atom array, with nodes representing atom sites, which is not constrained by blockade radius.

addition of extra Rz gates on qubits before and after the decomposition. Eqn. (6)-(13) may give Rz angles with absolute value greater than π . To reduce duration, these should be converted to the equivalent rotation amount with absolute value less than π by adding or subtracting multiples of 2π .

3.4 Post-Processing

While the steps presented in 3.2 and 3.3 are sufficient to convert a circuit into the NeutralAtomGateSet, there are additional steps we can take to further reduce gate count and total rotation amount. In particular, the axis of rotation of the GR gates can be changed from 0 to η at the cost of adding the gates $\prod_j \text{Rz}_j(\mp\eta)$ before ($-$) and after ($+$) the right-hand side of Eq. (5). This freedom in rotation axis can be used to eliminate some of the Rz gates that precede the first GR gate in the decomposition of U3 gates. Additionally, all Rz gates after the last GR gate in this decomposition can be eliminated by being “pushed forward” in the circuit and absorbed into the next layer of single-qubit gates.

3.5 Routing With Atom Movement

4. ROUTING PROCEDURE

4.1 Initial Mapping

The initial mapping assigns each *program qubit* (i.e., a qubit in the circuit) to a unique *hardware qubit* (i.e., a physical atom). The goal is to find an initial mapping that minimizes the number of operations that must be added via routing. This is typically achieved via heuristic methods that place frequently-interacting program qubits close together

on the hardware, often weighting interactions higher if they occur closer to the circuit’s start [6, 18, 23]. These prior works are effective for our compilation scheme.

4.2 Routing With SWAP Gates

4.2.1 Baseline SWAP-Based Routing

Routing consists of inserting operations into the circuit, often in the form of SWAP gates, to ensure the entire circuit can be executed while respecting the target architecture’s connectivity constraints. This process relies on the use of a *connectivity graph*, where nodes correspond to hardware qubits, and edges correspond to pairs of hardware qubits on which two-qubit gates can be executed. For each moment t in the circuit, we must satisfy the following constraint: $\forall \text{CZ}(q_a, q_b) \in t, (m_t(q_a), m_t(q_b)) \in E_{cg}$, where m_t is the mapping from program qubits to hardware qubits for moment t and E_{cg} is the connectivity graph’s edge set. If not satisfied, the mapping is permuted by inserting SWAP gates until the CZ gates’ operands are assigned to connected hardware qubits.

For our baseline routing strategy using SWAP gates, we follow the algorithm in [23], with the connectivity graph determined by constraints given below. Each SWAP gate is replaced with the decomposition in Figure 4.

4.2.2 Two-Qubit Gate Constraints on Neutral Atoms

On neutral atom hardware, connectivity is determined by Rydberg blockade radius: to execute a two-qubit gate, the distance between the qubits involved in that gate must be less than the blockade radius. The edge set of the connectivity graph contains all qubit pairs that satisfy this constraint.

Multiple two-qubit gates are parallelizable if 1) the gates act on disjoint subsets of qubits, and 2) operands of *different* gates are *farther* than a blockade radius—i.e., $\text{CZ}(q_a, q_b)$ and $\text{CZ}(q_c, q_d)$ can execute simultaneously if none of $\{(q_a, q_c), (q_a, q_d), (q_b, q_c), (q_b, q_d)\}$ are in the connectivity graph.

4.3 Routing With Atom Movement

4.3.1 Movement Constraints on Neutral Atoms

Unlike two-qubit SWAP and CZ gates, movement operations are not constrained by blockade radius. However, there are other considerations when routing with atom movement:

1. When moving from one location to another, an atom cannot get within some threshold distance d_{thr} from

any other (stationary or moving) qubits, where d_{thr} is the distance below which two adjacent optical traps significantly interfere with each other, resulting in a high probability of losing atomic qubits. This is not the same as the distance at which qubits experience crosstalk during gate execution, which determines spacing s .

2. If we label atoms' starting positions within the 2D array with coordinates (x, y) and ending coordinates (x', y') , simultaneous movement operations can occur on atoms with the same x value only if it will also result in the same x' value. Stated more simply, columns of atoms move horizontally together.
3. Similarly, we can simultaneously move atoms with the same y value only if they end at the same y' value, i.e., rows of atoms must move vertically together.

The last two constraints, depicted in Figure 6(a) and 6(b), are a consequence of the AOD technology used to move atoms, which can only create rectangular arrays of optical traps. However, when moving atoms one at a time, any arbitrary movement path can be completed; thus, if two movement operations do not meet these AOD-related constraints for parallel movement, they are scheduled in serial. This serialization often does not have significant effect on circuit duration, as 1) in the case of routing, opportunities for parallelism of movement operations are related to opportunities for parallelism of two-qubit gates, which are already low in many quantum circuits, and 2) if necessary, we can tailor our routing approach to these constraints. We address the first point, related to atom separation during movement, in 4.3.4.

Our routing algorithm assumes AOD rows and columns can cross—specifically when two atoms are simultaneously being moved in opposite directions without otherwise breaking these constraints. While this is feasible, it may lower fidelity on some hardware [4]. If this is an issue on the given hardware, we can make small adjustments to our algorithm without losing much of the improvements observed here. A simple solution is to move the two atoms in parallel up to the point where the AOD beams are close enough that atom loss or reduced fidelity is a risk, then move the first atom past the other while keeping the second atom stationary (allowing us to turn off the associated AOD beam), then move both in parallel the rest of the way. This will cause circuit duration to increase, though not by a significant amount, without any significant changes to the fidelity results simulated in this work. As a more sophisticated approach, we can develop mapping and routing algorithms aimed at minimizing crossings of rows and columns. We leave this for future work.

4.3.2 Naive Movement Algorithm

As a naive approach to routing with atom movement, we start by inserting SWAP gates into the circuit via the same steps described in 4.2. Then, instead of replacing each $\text{SWAP}(q_a, q_b)$ with a decomposition (4), we replace it with two atom movement operations that can execute in parallel: one to move q_a to atom site $m_t^{-1}(q_b)$ and another to move q_b to atom site $m_t^{-1}(q_a)$, where m_t^{-1} is the inverse of m_t . We determine which movement operations can be executed in parallel, according to constraints 2 and 3 in 4.3.1.

There is a subtle difference here in how the mapping is defined: instead of mapping program qubits to *hardware qubits*, we now map *program qubits* (whose states are stored by the same hardware qubits throughout circuit execution) to *atom sites*. We update our definition of the *connectivity graph* such that nodes are atom sites, and an edge exists between a pair of atom sites if a two-qubit gate can be performed on program qubits mapped to those sites.

4.3.3 Improved Movement Algorithm

When routing with movement operations instead of SWAP gates, our choice of which qubit pairs to permute in the mapping is not limited by blockade radius. This allows for much greater flexibility when making routing decisions.

Our algorithm relies on a simple yet powerful adjustment to the naive movement approach. We define a *movement graph*, shown in figure 5, where nodes are atom sites, an edge (s_i, s_j) indicates that an atom can be moved directly between sites s_i to s_j without breaking constraint 1 in 4.3.1, and edge weights give the distance between the corresponding atom sites. When iterating through the circuit, upon reaching a gate $\text{CZ}(q_a, q_b)$ that cannot be executed with the current mapping, we now use the *movement graph* instead of the *connectivity graph* to determine which qubits to permute in the mapping. We consider all pairs of program qubits (u, v) such that 1) $(m_{t-1}(u), m_{t-1}(v)) \in E_{mg}$ where E_{mg} is the movement graph's edge set, 2) $u \in \{q_a, q_b\}$ or $v \in \{q_a, q_b\}$, and 3) moving u to $m_{t-1}(v)$ and v to $m_{t-1}(u)$ will bring q_a and q_b closer than in the current mapping. Of these, we choose the program qubit pair (u', v') that results in the smallest distance between q_a and q_b after switching the places of u' and v' , i.e., after permuting the mapping such that $m_t(u') = m_{t-1}(v')$ and $m_t(v') = m_{t-1}(u')$. We break any ties in the same way as before. Importantly, throughout this algorithm, the *connectivity graph*, not the movement graph, still determines whether a CZ gate can execute between two qubits.

This approach increases average movement distance per operation but requires far fewer total operations, resulting in lower total movement distance and thereby reducing circuit runtime and amount of idle errors. Additionally, without long chains of SWAP gates, there is less disruption to the mappings of other qubits.

4.3.4 Adjusting Atom Placements

Routing with atom movement frequently requires us to switch the places of two atoms: the equivalent of a $\text{SWAP}(q_a, q_b)$ gate is replaced with moving q_a to $m(q_b)$ and q_b to $m(q_a)$, which we will label as $\text{Switch}(q_a, q_b)$. However, if we assume an evenly-spaced grid-like positioning of atom sites, executing this operation breaks condition 1 in 4.3.1, and executing the two movement operations in serial does not fix the issue. To solve this problem, we take advantage of the fact that neutral atom arrays allow for any arbitrary arrangement of sites, while still maintaining the rectangular structure required by the AOD. To switch the locations of atoms, we can “displace” one atom in the pair from its evenly-spaced grid point by d_{thr} , as shown in 6(c).

Our goal is to find an initial atom array configuration (i.e., initial set of “displacements” assigned to the qubits) that allow us to execute as many Switch operations as possible before needing to insert extra movement operations to adjust

displacements mid-circuit. We iterate through the list of `Switch` operations determined by the algorithm in 4.3.3 and decide displacements in the manner shown in 6(c) and 6(d).

For simplicity with this example, each displaced atom in Figure 6 is shifted diagonally (up and right) from the grid point. To achieve more flexibility, if possible without breaking atom movement constraints, we may choose to displace in only one direction: if the two qubits are in the same *row*, one must be displaced *up*; if in the same *column*, one must be displaced *right*. To ensure atom sites are no closer than $s - d_{thr}$, we do not allow displacement *down* or to the *left*, and we choose spacing s such that $s - d_{thr}$ is no smaller than the distance at which crosstalk begins to occur. Additionally, we may adjust movement distance of the `Switch` operation instead of adjusting initial displacements. E.g., in Figure 6(c), $q7$ could be moved a *shorter* distance so that it is vertically aligned with the grid point after executing `Switch`($q7, q8$), allowing us to execute `Switch`($q7, q8$) without the changes described in 6(d). If achieving this effect requires moving *farther*, it usually is better to adjust initial displacements.

5. METRICS

5.1 Calculating Circuit Duration

For a given neutral atom hardware model, we define the following values, given in Section 6: CZ gate duration, $Rz(\pi)$ gate duration, $GR(\pi, \phi)$ duration, and atom movement speed. For each single-qubit gate, duration is scaled by rotation amount; i.e., $t_\gamma = t_\pi \cdot \gamma/\pi$, where t_γ and t_π are the times required for rotations by angles γ and π , respectively. The duration of each atom movement operation is equal to the distance traveled divided by the movement speed.

Once the circuit has been routed and decomposed into the `NeutralAtomGateSet`, the circuit structure is naturally split into a) columns of parallel Rz gates, b) GR gates that are each applied to all qubits, and c) groups of CZ gates. Within each group of CZ gates and movement operations, we must determine which of these can execute in parallel, according to constraints specified in 4.2.2 and 4.3.1.

The duration of each moment, where a moment is a group of gates executed in parallel, is equal to the duration of the longest gate within that moment. The total circuit duration is calculated by summing over the durations of all moments.

Note that dead time between pulses – an experimental limitation on how quickly control devices can be switched – is about 15ns [11], approximately two orders of magnitude shorter than most neutral atom gate durations. Therefore, effects on circuit duration and idle errors from dead time are negligible and do not need to be considered. Also note that, in this case, there is not significant benefit from more sophisticated scheduling techniques than the layer-by-layer approach (such as those in [15]). This is because of the large number of GR gates in circuits decomposed to the `NeutralAtomGateSet`; even if a gate finishes earlier than other gates in the same moment, we still must wait until all gates in the moment have completed before executing the GR gate, since it is applied to all qubits in the circuit.

5.2 Noise Simulation

To evaluate fidelity of the quantum circuits produced by

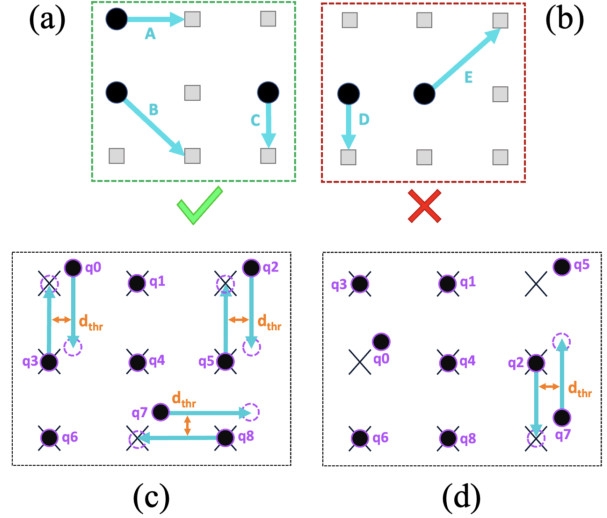


Figure 6: Examples of (a) allowed and (b) disallowed parallel movement operations. A and B are in the same *column* and move in the same direction *horizontally*, while B and C are in the same *row* and move in the same direction *vertically*; all three movement operations can be performed simultaneously. D and E are in the same row but move in *different* vertical directions; these operations must be scheduled in series. (b) If the first `Switch` operations are between pairs ($q0, q3$), ($q2, q5$), and ($q7, q8$), we can arbitrarily choose $q0, q2$, and $q7$ to “displace” off the evenly-spaced grid points (marked with black X’s), thus allowing the `Switch` operations to execute without breaking constraints. (c) If the next `Switch` is between ($q2, q7$), we update initial displacements such that $q5$ instead of $q2$ is displaced, allowing both `Switch`($q2, q5$) and `Switch`($q2, q7$) to execute with no extra cost.

our compiler, we use the trajectory method with a Pauli noise model [5] adapted to neutral atom hardware-level details.

We model two types of errors:

1. **Gate errors** occur from imperfections in the laser or microwave pulses used to implement gates (e.g., variations in Rabi frequency) or from atomic decay processes due to the finite lifetime of the Rydberg state or off-resonant scattering from the intermediate state. We make the common approximation that possible single-qubit gate errors are sampled from $\{no\ error\ (identity\ matrix),\ bit\ flip\ error\ (\sigma_x),\ phase\ flip\ error\ (\sigma_z),\ bit\ and\ phase\ flip\ error\ (\sigma_y)\}$ and two-qubit gate errors from $\mathcal{P}^{\otimes 2}$, randomly drawing an error for each gate in the circuit. The probabilities of drawing an error on a single-qubit and two-qubit gate are given, respectively, by p_{1k} and p_{2k} for $k \in \{X, Y, Z\}$, and probabilities of drawing no error are $1 - \sum p_{1k}$ and $1 - \sum p_{2k}$, where $p_{1x} = p_{1y} = 0.1\%$, $p_{1z} = 0.4\%$, $p_{2x} = p_{2y} = 0.2\%$ and $p_{2z} = 0.5\%$ [4].
2. **Idle errors** occur from unwanted interactions with the environment causing qubit states to decohere. *Amplitude damping*, related to the device’s T_1 time, describes

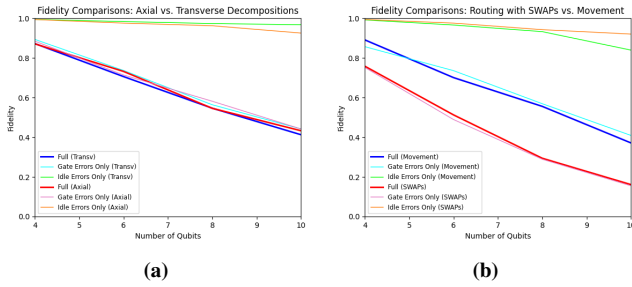


Figure 7: Fidelity plots comparing (a) decomposition methods and (b) routing methods for Cuccaro on A1. Other benchmarks show similar trends in fidelity. Fidelity decreases are mainly due to gate errors, rather than idle errors, consistent with what we would expect on neutral atom computers. Each data point is generated trajectory simulation with 1000 Haar random initial states. The curves for full noise simulation and gate error only simulation for the same strategy (Movement, SWAPs, Baseline, etc.) are insignificant, indicating that decoherence errors do not contribute significantly to loss in expected fidelity.

relaxation from a higher to lower energy level. *Dephasing* describes loss of relevant phase information (i.e., undesired rotations about the Bloch sphere’s z-axis) and is related to the T_2 and T_2^* times. Because the effects of dephasing in neutral atoms significantly dominate those of amplitude damping [17], at each moment we apply $(1 - \exp(-t/T_2^*))\sigma_z$ where t is the duration of the moment, determined by the longest gate in the moment.

Experimental work [4] clearly demonstrates that, at the movement speed which we assume, movement operations incur no decrease in fidelity nor loss of atoms. Thus, each atom movement operation in the circuit is subjected to an idle error but not a gate error. When not being moved, atoms can survive on the order of ~ 10 seconds before being lost; for the circuit sizes we study in this work, the rate at which we lose atoms is negligible, particularly compared to the rate at which we lose quantum information due to decoherence. Other sources of error – e.g., thermal motion of atoms, imperfect laser polarization, off-resonant scattering from the intermediate state in the two-photon Rydberg excitation – are accounted for in our gate error probabilities and do not need to be modeled separately.

6. EVALUATION METHODS

We evaluate our compiler methods on six different benchmarks, which are chosen to be reflective of relevant quantum computing programs. These include subroutines (multi-controlled X gate decomposition CNX and Greenberger-Horne-Zeilinger State Generator GHZ), arithmetic circuits (Cuccaro Adder Cuccaro and Quantum Fourier Transform QFT), and promising applications (Quantum Variational Optimization Algorithms VQAOA and Hamiltonian Simulation HamSim). We use scalable implementations found in [13,25]

Additionally, we evaluate our approaches on two different hardware models, representing different possible technical specifications for a real atomic system. In the first hardware

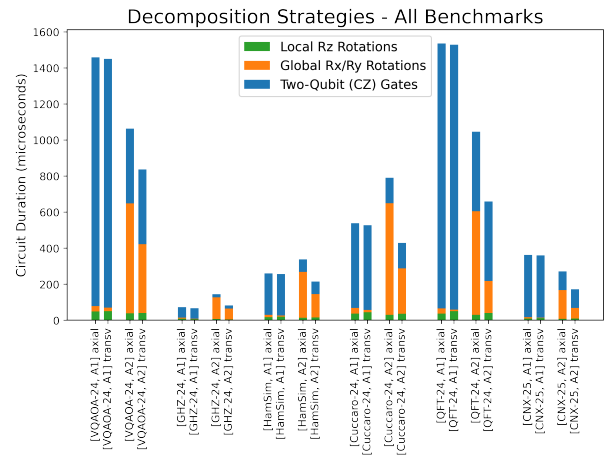


Figure 8: Comparing the transverse and axial decompositions for all benchmarks. We use circuit size of $n = 24$ for all circuits except CNX; for CNX we use $n = 24$, as this benchmark only allows for odd numbers of qubits.

model (A1), the duration of an Rz gate is equal to the duration of a GR gate of the same rotation amount, both of which are shorter than the duration of a two-qubit gate: durations of $Rz(\pi)$, $GR(\pi, \phi)$, and CZ gates are $0.25\mu s$, $0.25\mu s$, $2.5\mu s$, respectively [4]. In the second hardware model (A2), global gates dominate gate execution times, compared to both two-qubit and local Rz gates: durations of $Rz(\pi)$, $GR(\pi, \phi)$, and CZ gates are $0.2\mu s$, $5\mu s$, $0.75\mu s$, respectively [11]. The first is representative of laser control for both local and global gates, while the second is representative of laser control for local gates combined with microwave control for global gates. We do not need to consider the case in which Rz gate durations are dominant, as this is unlikely to occur in hardware.

We run our compiler algorithms with all possible benchmark and hardware combinations and, to demonstrate scalability of our compiler, vary the number of qubits in the circuit from $n = 10$ to $n = 70$. To convert to the StandardGateSet, we use Qiskit’s `transpile` function with basis gates {U3, CZ} [1]. To find an initial mapping, we use t[ket)’s `LinePlacement` method [6].

After applying our compiler pipeline steps, we compute the fidelity and total duration of the final circuit as described in Section 5. When simulating noise, we decrease all error probabilities by a factor of 10x from the values given in 5.2, allowing us to better distinguish fidelity results between the different compiler methods. Since gate error rates and coherence lifetimes will improve as the hardware develops, this is equivalent to simulating noise for quantum computers several years in the future. We assume a T_2^* time of 4ms [4].

Unless otherwise stated—e.g., when evaluating the impact of varying such parameters—we assume a $7\mu m$ blockade radius, $5\mu m$ spacing between atom sites, d_{thr} of $1\mu m$, and $0.55\mu m/\mu s$ movement speed [4, 11, 21]. In section 7.4, we study the effect of different blockade radii and spacing.

7. RESULTS & DISCUSSION

7.1 Decompositions to Native Gate Set

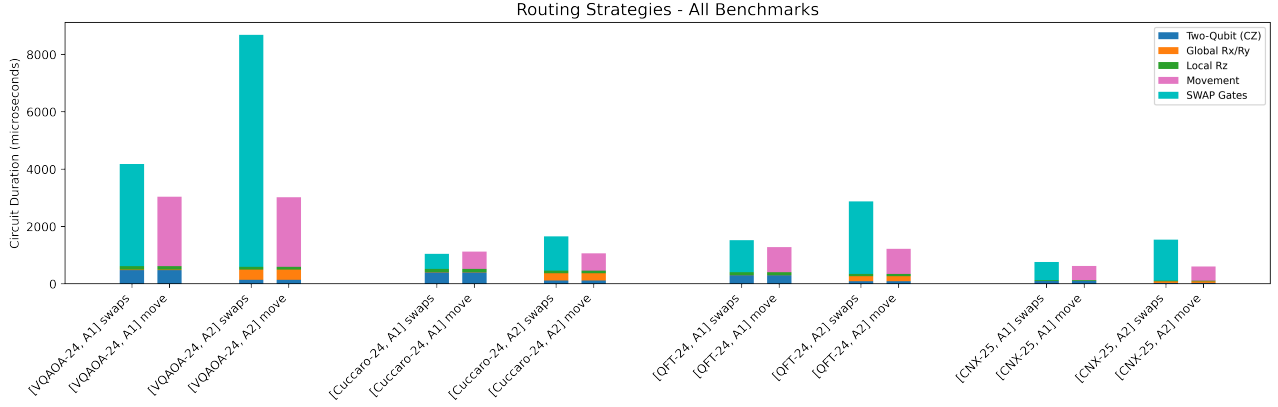


Figure 9: Comparing SWAP-based routing to the movement-based routing strategy we present in this work. As in Figure 8, we use $n = 25$ for CNX and $n = 24$ for all other benchmarks. For these plots, we use axial decomposition; note that choice of decomposition strategy does not impact routing overhead as our decompositions act only on single-qubit gates. For benchmarks GHZ and HamSim, an initial mapping could be found such that no routing operations were required.

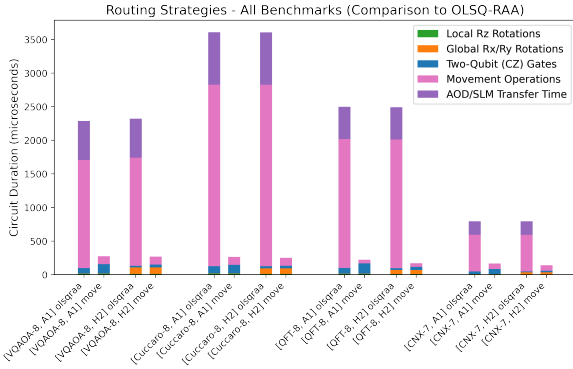


Figure 10: Comparing the OLSQ-RAA [24] routing method to our movement-based routing approach. We assume $20\mu\text{s}$ [3] for a transfer between AOD and SLM traps, which occurs in the OLSQ-RAA algorithm.

Because our work is the first to address decomposing into the `NeutralAtomGateSet`, there does not exist a reasonable baseline from prior work to which to compare our methods. Here, we compare the optimized decomposition method (transverse) to the unoptimized version (axial).

7.1.1 Circuit Duration

Compared to the axial decomposition method, the transverse decomposition method achieves up to 3.5x reduction in total global gate pulse durations and up to 2.9x reduction in time spent executing single-qubit gates (GR and Rz). As shown in 8, this is especially important on H1, where GR durations dominate gate execution time costs.

For some of the circuits—namely QFT, Cuccaro, and CNX—the Rz cost is lower with axial decompositions. This is because, when the Euler-angle decomposition in equation (4) is applied to a single-qubit gate with rotation angle of $\pi/2$ or π (which occurs frequently in QFT, Cuccaro, and CNX), at least one of the resulting θ , ϕ , or λ values is zero. These θ , ϕ , and λ become the rotation amounts of the Rz gates in

the axial decomposition, and a Rz with rotation angle of zero is equivalent to no gate. In comparison, when equations (6)-(13) are applied for the transverse decomposition, the Rz gate rotation angles are typically all nonzero.

However, this difference in Rz costs is small compared to the improvement in GR costs with transverse decompositions, and transverse therefore has better overall circuit duration for all benchmarks and hardware combinations.

Since these decompositions act only on moments containing single-qubit gates, the two-qubit gate costs are identical for both decomposition strategies.

7.1.2 Fidelity

As shown in Figure 7a, there is no noticeable difference in circuit fidelity between the axial and transverse decomposition strategies. While differences in circuit duration between the two decomposition strategies lead to slightly different idle error amounts, this difference is negligible.

7.2 Routing via Atom Movement

The largest amount of improvement in our compiler is achieved with the routing step. We compare our strategy using atom movement, described in 4.3.3, to 1) the baseline algorithm [6] using decomposed SWAP gates, discussed in 4.3.3 and 2) the OLSQ-RAA compiler [24].

7.2.1 SWAP-Based Comparison: Circuit Duration

The improvements from routing with atom movement come from the fact that a single SWAP gate must be decomposed into 21 gates from the `NeutralAtomGateSet`, as shown in Figure 4, to be executed on neutral atom hardware. This requires $10.5\mu\text{s}$ and $24\mu\text{s}$ per SWAP on hardware A1 and A2, respectively. In comparison, a single SWAP implemented via movement operations requires $9\mu\text{s}$, assuming atom spacing of $5\mu\text{m}$. Thus, in almost all cases, and due to factors discussed in 4.3.3, routing via atom movement will result in speedup. It is possible for the total circuit duration using movement routing to exceed the baseline, due to the added movement operations described in 4.3.4 or differences in parallelism opportunities between SWAP gates

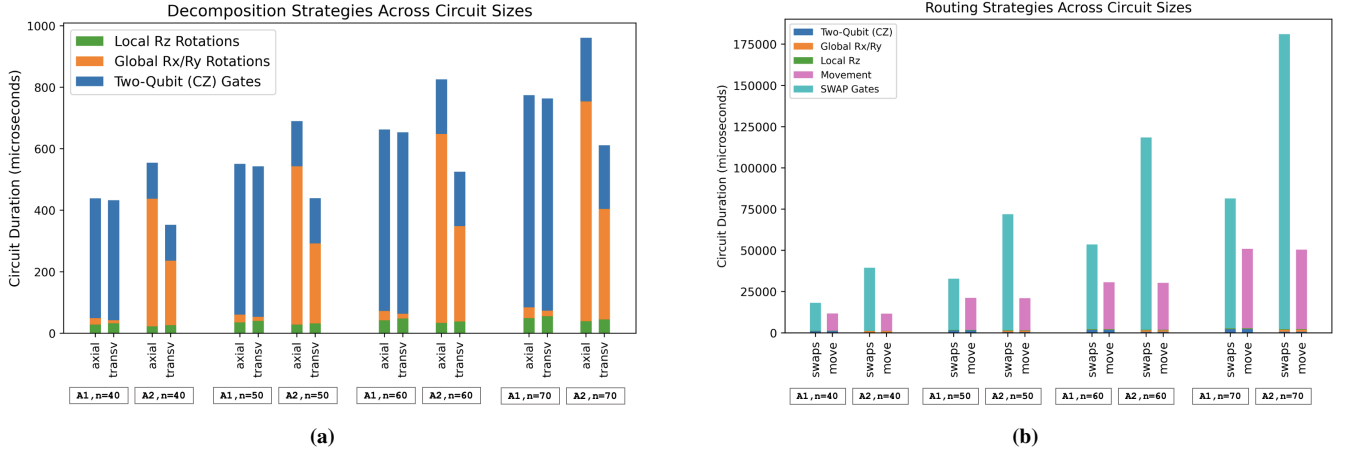


Figure 11: Scaling of (a) decomposition strategies for HamSim and (b) routing algorithms for VQAOA. We test circuit sizes ranging from $n = 40$ to $n = 70$ for blockade radius of $7\mu\text{m}$ and spacing of $5\mu\text{m}$. For all n in this plot, speedup from routing remained around 2.5x and improvement in global gate execution time remained around 2.4x, demonstrating that the conclusions drawn from our experiments do not change as circuit size increases.

and movement operations. However, we only observe this with Cuccaro on A1. For A2, every benchmark achieved significant speedup when atom movement is used for routing.

7.2.2 SWAP-Based Comparison: Fidelity

All benchmarks, on both models, saw immense improvement in fidelity, as shown in Figure 7b. This is because each of the 21 gates in the SWAP decomposition can potentially cause gate errors, which are the main source of error on neutral atom devices. In the majority of cases, routing with atom movement will also lead to fewer idle errors due to shorter circuit durations. In the single case where circuit duration is longer when using atom movement (Cuccaro on A2), the slightly higher idle errors relative to the baseline is negligible compared to the lower amount of gate errors (Figure 7b).

7.2.3 OLSQ-RAA Comparison: Circuit Duration

Compared to the OLSQ-RAA compiler [24], we achieve 10x average speedup across all benchmarks for the circuit sizes shown in Figure 10. This improvement stems primarily from the large space requirements for OLSQ-RAA, meaning that atoms must be moved much farther distances, thus taking more time. OLSQ-RAA focuses primarily on minimizing costs due to two-qubit gates, without fully accounting for or optimizing atom movement overheads. Also, OLSQ-RAA’s approach relies on transferring atoms between AOD and SLM traps mid-circuit. Each transfer can take 20-50 μs or longer [3, 4], and this cost can add up. Our approach assumes all atoms remain in AOD traps throughout circuit execution, eliminating the need for transfer times.

As shown by the blue bars in Figure 10, OLSQ-RAA achieves lower two-qubit gate time costs. This is due to differences in parallelism, as both approaches require the same number of two-qubit gates; neither approach adds gates from the unrouted circuit since routing is achieved via atom movement. Achieving this extra parallelism while respecting constraints (see Section 4.2.2), however, requires higher atom movement cost; if qubits of different CZ gates have overlap-

ping blockade radii, we find it is better to serialize the CZ gates than to incur the cost of moving qubits apart.

7.2.4 OLSQ-RAA Comparison: Fidelity

We expect gate errors to be the same, as both approaches have the same number of gates (as mentioned above). We expect idle errors to be slightly worse for OLSQ-RAA due to longer circuit durations. We note that OLSQ-RAA may have slightly better fidelity because it prevents crossings of AOD rows and columns, which can cause some additional heating, though it is unclear how much of an effect this will have. For more details on heating during atom movement, we refer the reader to [4].

7.3 Scalability

7.3.1 Results for Increased Circuit Sizes

Figure 11 shows the effects of scaling up the size of circuits. As the number of qubits in the circuit grows, the qualitative results—which compiler strategies are better in which contexts—remain unchanged. With bigger circuits, particularly as circuit duration approaches device coherence time, it becomes increasingly more important to optimize the compiler steps in the ways discussed in this paper.

7.3.2 Compilation Overhead & Complexity Analysis

The decomposition steps presented in 3.2 and 3.3 are linear in the number of gates in the circuit, and the additional post-processing steps and optimizations discussed in 3.4 do not further increase complexity. The routing algorithms provided in 4.3 have the same complexity as the baseline SWAP-based approach from [6, 23]; incorporating movement into routing does not worsen compilation overhead. If necessary, other SWAP-based routing approaches with lower complexity than [6, 23] can easily be adapted to incorporate atom movement by following the same approach presented in our work.

7.4 Effect of Hardware-Level Parameters

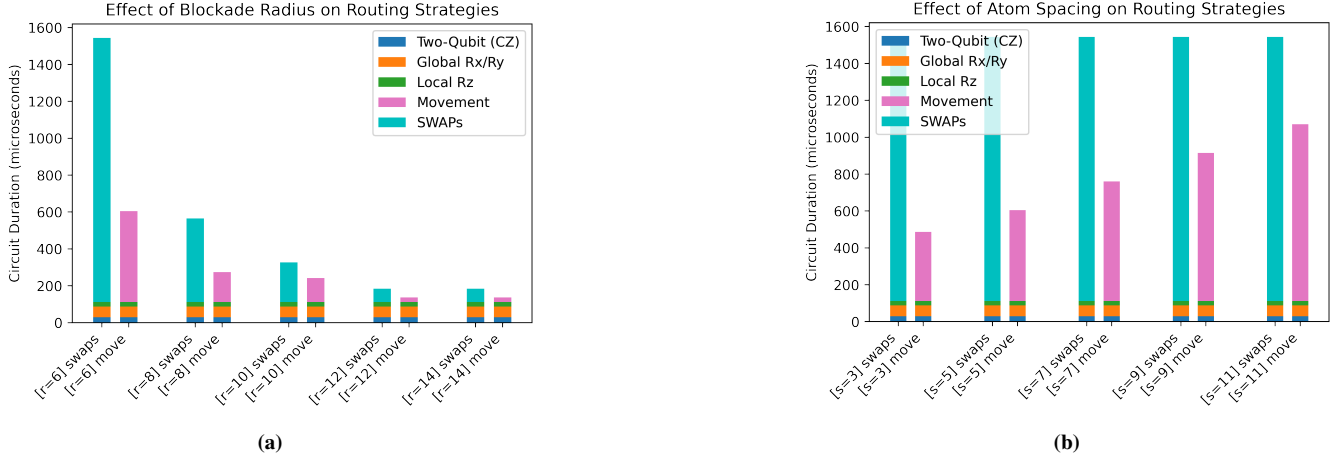


Figure 12: (a) Effect of blockade radius (in μm) on mapping strategies for CNX circuits with atom spacing of $5\mu\text{m}$. The first pair of bars is for nearest-neighbor-only connectivity, the second includes nearest neighbor and closest diagonal connections, etc. (b) Effect of atom spacing (in μm), again for benchmark CNX, and with a blockade radius of $1\mu\text{m}$ greater than the given spacing, which gives nearest-neighbor-only connectivity for all atom spacings. For both (a) and (b), similar qualitative trends were observed across all benchmarks, with the greatest quantitative impact seen in benchmarks requiring the most routing operations. Note that blockade radius and spacing do not impact decomposition results.

7.4.1 Effect of Blockade Radius

Shown in Figure 12a, we study the effect of increasing blockade radius within the range of $r_b = 5\mu\text{m}$ to $r_b = 15\mu\text{m}$, which is currently supported by neutral atom hardware [8]. With greater r_b , and thus higher connectivity, fewer SWAP gates (or the equivalent movement operations) are needed to make the circuit’s CZ gates executable, leading to improved results for both routing approaches. With both, there is also a decrease in two-qubit gate parallelism with increasing r_b , as this makes it more likely that operands of different CZ gates will have overlapping blockade radii. However, for the majority of circuits, the decrease in SWAP gates or movement operations far outweighs any loss in two-qubit parallelism.

In Figure 12a, we also observe that, as r_b increases, the cost of routing with the SWAP gate decomposition approaches the cost of routing with movement. This results from a greater number of edges in the connectivity graph (determining SWAP insertion) without impacting the number of edges in the movement paths graph (determining Switch insertion). Stated less abstractly, larger r_b grants more flexibility with routing decisions when using SWAP gates, which was already present with movement routing at lower r_b .

This indicates that movement allows us to achieve some of the benefits of a larger blockade radius, while in reality keeping the blockade radius relatively small. One huge advantage of this is that we can avoid the greater two-qubit gate error rates that occur when accessing higher Rydberg energy levels necessary to implement a larger blockade radius [9].

7.4.2 Effect of Atom Spacing

Figure 12b shows the impact of varying spacing s between atom array sites. As with blockade radius, we choose a range based on recent hardware research: $s = 3\mu\text{m}$ to $s = 11\mu\text{m}$. To isolate the effect of spacing from the effect of connectivity, we set $r_b = s + 1\mu\text{m}$ (note we need $r_b > s$, otherwise there would exist no pairs of qubits on which a CZ gate could be

executed). As expected, since movement time is proportional to distance, the cost of routing with movement increases with larger spacing. With most of the circuits, routing with movement still performed better than the baseline (in terms of both circuit duration and fidelity) even at the largest s tested.

Though spacing does not effect gate durations—thus leaving the time overhead unchanged when routing with the SWAP gate decomposition—larger spacing will require a greater blockade radius to execute the CZ gates. As mentioned in 7.4.1, this will lead to higher two-qubit gate error rates.

7.4.3 Adapting to Hardware Specifications

The exact amount of speedup we achieve with movement will depend on the chosen r_b and s , which may depend on the hardware device. With s , we want the smallest value that does not lead to non-negligible increases in crosstalk. With r_b , we want the largest value – leading to highest connectivity – that does not significantly decrease two-qubit gate fidelity.

8. CONCLUSION

We present a compiler that converts a circuit into a realistic neutral atom gate set, in which Rx and Ry rotations can only be implemented globally. This step is essential to be able to execute circuits on current hardware. To overcome expensive single-qubit decompositions involving global gates, we specifically optimize rotation amount of GR and Rz gates. As an alternative to expensive SWAP decompositions, we propose routing strategies involving atom movement operations. Together, these approaches achieve significant improvement in circuit duration and fidelity. We demonstrate that our compiler passes are effective for a wide variety of hardware specifications and hardware-level parameter values, which is of great importance as neutral atom hardware technologies continue to develop and evolve.

ACKNOWLEDGMENTS

This work is funded in part by EPIQC, an NSF Expedition in Computing, under award CCF-1730449; in part by STAQ under award NSF Phy-1818914; in part by the US Department of Energy Office of Advanced Scientific Computing Research, Accelerated Research for Quantum Computing Program; and in part by the NSF Quantum Leap Challenge Institute for Hybrid Quantum Architectures and Networks (NSF Award 2016136) and in part based upon work supported by the U.S. Department of Energy, Office of Science, National Quantum Information Science Research Centers.

FTC is Chief Scientist for Quantum Software at Infleqtion and an advisor to Quantum Circuits, Inc.

REFERENCES

[1] M. S. ANIS, Abby-Mitchell, H. Abraham, AduOffei, R. Agarwal, G. Agliardi, M. Aharoni, V. Ajith, I. Y. Akhalwaya, G. Aleksandrowicz, T. Alexander, M. Amy, S. Anagolum, Anthony-Gandon, E. Arbel, A. Asfaw, A. Athalye, A. Avkhadiev, C. Azaustre, P. Bhole, A. Banerjee, S. Banerjee, W. Bang, A. Bansal, P. Barkoutsos, A. Barnawal, G. Barron, G. S. Barron, L. Bello, Y. Ben-Haim, M. C. Bennett, D. Bevenius, D. Bhatnagar, P. Bhatnagar, A. Bhohe, P. Bianchini, L. S. Bishop, C. Blank, S. Bolos, S. Bopardikar, S. Bosch, S. Brandhofer, Brandon, S. Bravyi, N. Bronn, Bryce-Fuller, D. Bucher, A. Burov, F. Cabrera, P. Calpin, L. Capelluto, J. Carballo, G. Carrascal, A. Carriker, I. Carvalho, A. Chen, C.-F. Chen, E. Chen, J. C. Chen, R. Chen, F. Chevallier, K. Chinda, R. Cholarajan, J. M. Chow, S. Churchill, CisterMoke, C. Claus, C. Clauss, C. Clothier, R. Cocking, R. Cocuzzo, J. Connor, F. Correa, Z. Crockett, A. J. Cross, A. W. Cross, S. Cross, J. Cruz-Benito, C. Culver, A. D. Córcoles-Gonzales, N. D. S. Dague, T. E. Dandachi, A. N. Dangwal, J. Daniel, M. Daniels, M. Dartialh, A. R. Davila, F. Debouni, A. Dekusar, A. Deshmukh, M. Deshpande, D. Ding, J. Doi, E. M. Dow, P. Downing, E. Drechsler, E. Dumitrescu, K. Dumon, I. Duran, K. EL-Safty, E. Eastman, G. Eberle, A. Ebrahimi, P. Eendebak, D. Egger, ElePT, Emilio, A. Espiricueta, M. Everitt, D. Facoetti, Farida, P. M. Fernández, S. Ferracin, D. Ferrari, A. H. Ferrera, R. Fouilland, A. Frisch, A. Fuhrer, B. Fuller, M. GEORGE, J. Gacon, B. G. Gago, C. Gambella, J. M. Gambetta, A. Gammanpila, L. Garcia, T. Garg, S. Garion, J. R. Garrison, J. Garrison, T. Gates, H. Georgiev, L. Gil, A. Gilliam, A. Giridharan, Glen, J. Gomez-Mosquera, Gonzalo, S. d. I. P. González, J. Gorzinski, I. Gould, D. Greenberg, D. Grinko, W. Guan, D. Guijo, J. A. Gunnels, H. Gupta, N. Gupta, J. M. Günther, M. Haglund, I. Haide, I. Hamamura, O. C. Hamido, F. Harkins, K. Hartman, A. Hasan, V. Havlicek, J. Hellmers, \ Herok, S. Hillmich, H. Horii, C. Howington, S. Hu, W. Hu, C.-H. Huang, J. Huang, R. Huisman, H. Imai, T. Imamichi, K. Ishizaki, Ishwor, R. Iten, T. Itoko, A. Ivrii, A. Javadi, A. Javadi-Abhari, W. Javed, Q. Jianhua, M. Jivrajani, K. Johns, S. Johnstun, Jonathan-Shoemaker, JosDenmark, JoshDumo, J. Judge, T. Kachmann, A. Kale, N. Kanazawa, J. Kane, Kang-Bae, A. Kapila, A. Karazeev, P. Kassebaum, T. Kehrer, J. Kelso, S. Kelso, H. v. Kemenade, V. Khanderao, S. King, Y. Kobayashi, Kovi11Day, A. Kovyshin, R. Krishnakumar, P. Krishnamurthy, V. Krishnan, K. Krsulich, P. Kumkar, G. Kus, R. LaRose, E. Laca, R. Lambert, H. Landa, J. Lapeyre, J. Latone, S. Lawrence, C. Lee, G. Li, T. J. Liang, J. Lishman, D. Liu, P. Liu, Lolcroc, A. K. M, L. Madden, Y. Maeng, S. Maheshkar, K. Majmudar, A. Malyshev, M. E. Mandouh, J. Manela, Manjula, J. Marecek, M. Marques, K. Marwaha, D. Maslov, P. Maszota, D. Mathews, A. Matsuo, F. Mazhandu, D. McClure, M. McElaney, C. McGarry, D. McKay, D. McPherson, S. Meesala, D. Meirum, C. Mendell, T. Metcalfe, M. Mevissen, A. Meyer, A. Mezzacapo, R. Midha, D. Miller, H. Miller, Z. Minev, A. Mitchell, N. Moll, A. Montanez, G. Monteiro, M. D. Mooring, R. Morales, N. Moran, D. Morcuende, S. Mostafa, M. Motta, R. Moyard, P. Murali, D. Murata, J. Müggenburg, T. NEMOZ, D. Nadlinger, K. Nakanishi, G. Nannicini, P. Nation, E. Navarro, Y. Naveh, S. W. Neagle, P. Neuweiler, A. Ngoueya, T. Nguyen, J. Nicander, Nick-Singstock, P. Niroula, H. Norlen, NuoWenLei, L. J. O’Riordan, O. Ogunbayo, P. Ollitrault, T. Onodera, R. Otaolea, S. Oud, D. Padilha, H. Paik, S. Pal, Y. Pang, A. Panigrahi, V. R. Pascuzzi, S. Perriello, E. Peterson, A. Phan, K. Pilch, F. Piro, M. Pistoia, C. Piveteau, J. Plewa, P. Pocreau, A. Pozas-Kerstjens, R. Pracht, M. Prokop, V. Prutyayov, S. Puri, D. Puzzuoli, Pythonix, J. Pérez, Quant02, Quintiii, R. I. Rahman,

A. Raja, R. Rajeev, I. Rajput, N. Ramagiri, A. Rao, R. Raymond, O. Reardon-Smith, R. M.-C. Redondo, M. Reuter, J. Rice, M. Riedemann, Rietesh, D. Risinger, P. Rivero, M. L. Rocca, D. M. Rodríguez, RohithKarur, B. Rosand, M. Rossmannek, M. Ryu, T. SAPV, N. R. C. Sa, A. Saha, A. A. Saki, S. Sanand, M. Sandberg, H. Sandesara, R. Sapra, H. Sargsyan, A. Sarkar, N. Sathaye, N. Savola, B. Schmitt, C. Schnabel, Z. Schoenfeld, T. L. Scholten, E. Schoute, M. Schultebrandt, J. Schwarm, J. Seaward, Sergi, I. F. Sertage, K. Setia, F. Shah, N. Shammah, W. Shanks, R. Sharma, Y. Shi, J. Shoemaker, A. Silva, A. Simonetto, D. Singh, D. Singh, P. Singh, P. Singkanipa, Y. Siraichi, Siri, J. Sistos, I. Sitdikov, S. Sivarajah, Slavikmew, M. B. Sletfjerd, J. A. Smolin, M. Soeken, I. O. Sokolov, I. Sokolov, V. P. Soloviev, SooluThomas, Starfish, D. Steenzen, M. Stypulkoski, A. Suau, S. Sun, K. J. Sung, M. Suwama, O. S\lowik, H. Takahashi, T. Takawale, I. Tavernelli, C. Taylor, P. Taylour, S. Thomas, K. Tian, M. Tillet, M. Tod, M. Tomasik, C. Tornow, E. d. I. Torre, J. L. S. Tournal, K. Trabing, M. Treinish, D. Trenev, TrishaPe, F. Truger, G. Tsilimigkounakis, D. Tulsi, D. Tuna, W. Turner, Y. Vaknin, C. R. Valcarce, F. Varchon, A. Vartak, A. C. Vazquez, P. Vijaywargiya, V. Villar, B. Vishnu, D. Vogt-Lee, C. Vuillot, J. Weaver, J. Weidenfeller, R. Wiecezorek, J. A. Wildstrom, J. Wilson, E. Winston, WinterSoldier, J. J. Woehr, S. Woerner, R. Woo, C. J. Wood, R. Wood, S. Wood, J. Wootton, M. Wright, L. Xing, J. YU, B. Yang, U. Yang, J. Yao, D. Yeralin, R. Yonekura, D. Yonge-Mallo, R. Yoshida, R. Young, J. Yu, L. Yu, Yuma-Nakamura, C. Zachow, L. Zdanski, H. Zhang, I. Zidar, B. Zimmermann, C. Zoufal, aeddins-ibm, alexzhang13, b63, bartek-bartlomiej, bcamorison, brandhsn, chetmurthy, deeplokhande, dekel.meirom, dime10, dlasecki, ehchen, ewinston, fanizzamarco, fs1132429, gadial, galeinston, georgezhou20, georgios-ts, gruu, hhorii, hhyap, hykavitha, itoko, jeppvinkel, jessica-angel7, jezerjo14, jliu45, johannesgreiner, jscott2, klinvill, krutik2966, ma5x, michelle4654, msuwama, nico-lgrs, nrhawkins, ntiwsvp, ordmoj, s. pahwa, pritamsinh2304, rithikaadiga, ryanocuzzo, saktar-unr, saswati-qiskit, septembrr, sethmerkl, sg495, shaashwat, smturro2, sternparky, strickroman, tigerjack, tsura-crisaldo, upsideon, vadebayo49, welien, willhbang, wmurphy-collabstar, yang.luh, and M. Čepulkovskis, “Qiskit: An Open-source Framework for Quantum Computing,” 2021.

[2] J. M. Baker, A. Litteken, C. Duckering, H. Hoffman, H. Bernien, and F. T. Chong, “Exploiting Long-Distance Interactions and Tolerating Atom Loss in Neutral Atom Quantum Architectures,” Nov. 2021, arXiv:2111.06469 [quant-ph]. [Online]. Available: <http://arxiv.org/abs/2111.06469>

[3] J. Beugnon, C. Tuchendler, H. Marion, A. Gaëtan, Y. Miroshnychenko, Y. R. P. Sortais, A. M. Lance, M. P. A. Jones, G. Messin, A. Browaeys, and P. Grangier, “Two-dimensional transport and transfer of a single atomic qubit in optical tweezers,” *Nature Physics*, vol. 3, no. 10, pp. 696–699, Oct. 2007, number: 10 Publisher: Nature Publishing Group. [Online]. Available: <https://www.nature.com/articles/nphys698>

[4] D. Bluvstein, H. Levine, G. Semeghini, T. T. Wang, S. Ebadi, M. Kalinowski, A. Keesling, N. Maskara, H. Pichler, M. Greiner, V. Vuletić, and M. D. Lukin, “A quantum processor based on coherent transport of entangled atom arrays,” *Nature*, vol. 604, no. 7906, pp. 451–456, Apr. 2022. [Online]. Available: <https://www.nature.com/articles/s41586-022-04592-6>

[5] T. A. Brun, “A simple model of quantum trajectories,” *American Journal of Physics*, vol. 70, no. 7, pp. 719–737, Jul. 2002. [Online]. Available: <http://aapt.scitation.org/doi/10.1119/1.1475328>

[6] A. Cowtan, S. Dilkes, R. Duncan, A. Krajenbrink, W. Simmons, and S. Sivarajah, “On the qubit routing problem,” p. 32 pages, 2019, arXiv:1902.08091 [quant-ph]. [Online]. Available: <http://arxiv.org/abs/1902.08091>

[7] C. Developers, “Cirq,” Dec. 2022, See full list of authors on Github: <https://github.com/quantumlib/Cirq/graphs/contributors>. [Online]. Available: <https://doi.org/10.5281/zenodo.7465577>

[8] S. Ebadi, A. Keesling, M. Cain, T. T. Wang, H. Levine, D. Bluvstein, G. Semeghini, A. Omran, J.-G. Liu, R. Samajdar, X.-Z. Luo, B. Nash, X. Gao, B. Barak, E. Farhi, S. Sachdev, N. Gemelke, L. Zhou, S. Choi, H. Pichler, S.-T. Wang, M. Greiner, V. Vuletić, and M. D. Lukin, “Quantum optimization of maximum independent set using rydberg atom arrays,” *Science*, vol. 376, no. 6598, pp. 1209–1215, 2022. [Online]. Available: <https://www.science.org/doi/abs/10.1126/science.abo6587>

[9] S. J. Evered, D. Bluvstein, M. Kalinowski, S. Ebadi, T. Manovitz, H. Zhou, S. H. Li, A. A. Geim, T. T. Wang, N. Maskara, H. Levine, G. Semeghini, M. Greiner, V. Vuletić, and M. D. Lukin, “High-fidelity parallel entangling gates on a neutral atom quantum computer,” 2023.

- [Online]. Available: <https://arxiv.org/abs/2304.05420>
- [10] T. M. Graham, M. Kwon, B. Grinkemeyer, Z. Marra, X. Jiang, M. T. Lichtman, Y. Sun, M. Ebert, and M. Saffman, "Rydberg mediated entanglement in a two-dimensional neutral atom qubit array," *Physical Review Letters*, vol. 123, no. 23, p. 230501, Dec. 2019, arXiv:1908.06103 [physics, physics:quant-ph]. [Online]. Available: <http://arxiv.org/abs/1908.06103>
- [11] T. M. Graham, Y. Song, J. Scott, C. Poole, L. Phuttitarn, K. Jooya, P. Eichler, X. Jiang, A. Marra, B. Grinkemeyer, M. Kwon, M. Ebert, J. Cherek, M. T. Lichtman, M. Gillette, J. Gilbert, D. Bowman, T. Ballance, C. Campbell, E. D. Dahl, O. Crawford, N. S. Blunt, B. Rogers, T. Noel, and M. Saffman, "Multi-qubit entanglement and algorithms on a neutral-atom quantum computer," *Nature*, vol. 604, no. 7906, pp. 457–462, Apr. 2022, number: 7906 Publisher: Nature Publishing Group. [Online]. Available: <https://www.nature.com/articles/s41586-022-04603-6>
- [12] D. Jaksch, J. I. Cirac, P. Zoller, S. L. Rolston, R. Cote, and M. D. Lukin, "Fast quantum gates for neutral atoms," *Physical Review Letters*, vol. 85, no. 10, pp. 2208–2211, Sep. 2000, arXiv:quant-ph/0004038. [Online]. Available: <http://arxiv.org/abs/quant-ph/0004038>
- [13] A. L. Jonathan M Baker, Casey Duckering, "quantumcircuitbenchmarks," Dec. 2020.
- [14] H. Levine, D. Bluvstein, A. Keesling, T. T. Wang, S. Ebadi, G. Semeghini, A. Omran, M. Greiner, V. Vuletić, and M. D. Lukin, "Dispersive optical systems for scalable raman driving of hyperfine qubits," *Phys. Rev. A*, vol. 105, p. 032618, Mar 2022. [Online]. Available: <https://link.aps.org/doi/10.1103/PhysRevA.105.032618>
- [15] Y. Li, Y. Zhang, M. Chen, X. Li, and P. Xu, "Timing-Aware Qubit Mapping and Gate Scheduling Adapted to Neutral Atom Quantum Computing," *IEEE Transactions on Computer-Aided Design of Integrated Circuits and Systems*, pp. 1–1, 2023, conference Name: IEEE Transactions on Computer-Aided Design of Integrated Circuits and Systems.
- [16] A. Molavi, A. Xu, M. Diges, L. Pick, S. Tannu, and A. Albarghouthi, "Qubit Mapping and Routing via MaxSAT," Aug. 2022, arXiv:2208.13679 [quant-ph]. [Online]. Available: <http://arxiv.org/abs/2208.13679>
- [17] M. Morgado and S. Whitlock, "Quantum simulation and computing with Rydberg-interacting qubits," *AVS Quantum Science*, vol. 3, no. 2, p. 023501, Jun. 2021, arXiv:2011.03031 [cond-mat, physics:physics, physics:quant-ph]. [Online]. Available: <http://arxiv.org/abs/2011.03031>
- [18] P. Murali, J. M. Baker, A. J. Abhari, F. T. Chong, and M. Martonosi, "Noise-Adaptive Compiler Mappings for Noisy Intermediate-Scale Quantum Computers," Jan. 2019, arXiv:1901.11054 [quant-ph]. [Online]. Available: <http://arxiv.org/abs/1901.11054>
- [19] T. Patel, D. Silver, and D. Tiwari, "Geyser: a compilation framework for quantum computing with neutral atoms," in *Proceedings of the 49th Annual International Symposium on Computer Architecture*. New York New York: ACM, Jun. 2022, pp. 383–395. [Online]. Available: <https://dl.acm.org/doi/10.1145/3470496.3527428>
- [20] M. Saffman, T. G. Walker, and K. Mølmer, "Quantum information with Rydberg atoms," *Reviews of Modern Physics*, vol. 82, no. 3, pp. 2313–2363, Aug. 2010.
- [21] P. Scholl, M. Schuler, H. J. Williams, A. A. Eberharter, D. Barredo, K.-N. Schymik, V. Lienhard, L.-P. Henry, T. C. Lang, T. Lahaye, A. M. Läuchli, and A. Browaeys, "Quantum simulation of 2D antiferromagnets with hundreds of Rydberg atoms," *Nature*, vol. 595, no. 7866, pp. 233–238, Jul. 2021, number: 7866 Publisher: Nature Publishing Group. [Online]. Available: <https://www.nature.com/articles/s41586-021-03585-1>
- [22] K. Singh, S. Anand, A. Pocklington, J. T. Kemp, and H. Bernien, "Dual-Element, Two-Dimensional Atom Array with Continuous-Mode Operation," *Physical Review X*, vol. 12, no. 1, p. 011040, Mar. 2022, publisher: American Physical Society. [Online]. Available: <https://link.aps.org/doi/10.1103/PhysRevX.12.011040>
- [23] S. Sivarajah, S. Dilkes, A. Cowtan, W. Simmons, A. Edgington, and R. Duncan, "tlket): a retargetable compiler for NISQ devices," *Quantum Science and Technology*, vol. 6, no. 1, p. 014003, Nov. 2020, publisher: IOP Publishing. [Online]. Available: <https://dx.doi.org/10.1088/2058-9565/ab8e92>
- [24] B. Tan, D. Bluvstein, M. D. Lukin, and J. Cong, "Qubit Mapping for Reconfigurable Atom Arrays," in *Proceedings of the 41st IEEE/ACM International Conference on Computer-Aided Design*, ser. ICCAD '22. New York, NY, USA: Association for Computing Machinery, Dec. 2022, pp. 1–9. [Online]. Available: <https://dl.acm.org/doi/10.1145/3508352.3549331>
- [25] T. Tomesh, P. Gokhale, V. Omole, G. S. Ravi, K. N. Smith, J. Vizslai, X.-C. Wu, N. Hardavellas, M. R. Martonosi, and F. T. Chong, "SupermarQ: A Scalable Quantum Benchmark Suite," in *2022 IEEE International Symposium on High-Performance Computer Architecture (HPCA)*, Apr. 2022, pp. 587–603, ISSN: 2378-203X.
- [26] M. Xu, Z. Li, O. Padon, S. Lin, J. Pointing, A. Hirth, H. Ma, J. Palsberg, A. Aiken, U. A. Acar, and Z. Jia, "Quartz: superoptimization of Quantum circuits," in *Proceedings of the 43rd ACM SIGPLAN International Conference on Programming Language Design and Implementation*. San Diego CA USA: ACM, Jun. 2022, pp. 625–640. [Online]. Available: <https://dl.acm.org/doi/10.1145/3519939.3523433>